Abstract:

Muons generated by cosmic rays constantly pass through the bodies of everyone on Earth. Using a QuarkNet DAQ board and a pair of plastic scintillator paddles, we show that we can detect cosmic ray muons, we measure the muon's mean lifetime at $\tau_\mu = (2.205 \pm 0.062)\mu$s, and we find that the vertical muon flux at Earth's surface is $(95\pm10)\text{s}^{-1}\text{m}^{-2}\text{sr}^{-1}$ and follows the expected $\cos^2\theta$ zenith-angle distribution. We also present a new method for muon telescope data analysis based on regularization methods.

# 1 Introduction & Objectives

Earth withstands a light barrage of extremely fast-moving particles called *cosmic rays*. Some of these barely make a mark on our atmosphere, while others slam into it with the kinetic energy of an apple moving at 60 miles per hour [2]. When higher-energy cosmic rays hit our atmosphere, they fragment into near-light speed showers of 'daughter' particles, including muons.

Muons are short-lived elementary particles nearly identical to electrons, but 200 times as massive. This additional mass allows them to keep their momentum through the atmosphere, and even traverse meters of solid rock.[1] These particles would normally decay before they reach the Earth's surface, but relativistic effects allow them to reach the ground at a rate of roughly 1 muon per square centimeter per minute.

In this lab, we aim to observe muons passing through a pair of scintillator detectors, then use these detectors to make measurements of the muon's lifetime and the amount of muons coming from different directions in the sky.

# 2 Theory

## 2.1 Cosmic Rays

Cosmic rays are high-energy particles (typically the electron-stripped nuclei of common atoms) accelerated by supernovae and active galactic nuclei.[2] These particles vary wildly in energy and flux: their energies can be anywhere from 1GeV to $10^{11}$GeV, and the flux at these energies spans an even wider range [1]. When these primary cosmic rays strike the Earth's atmosphere, they emit a shower of many daughter particles, including charged pions ($\pi^\pm$). From the standard model, the pion's mean lifetime is just 26ns [9], and their decay mode is dominated by the process following process (with a branching ratio $> 0.999$):

$$\pi^+ \to \mu^+ + \nu_\mu \tag{1}$$

$$\pi^- \to \mu^- + \bar{\nu}_\mu \tag{2}$$

The muons resulting from these decays have a much longer half life of $2.2\mu$s (as we will show in this report), and are massive enough to continue through to Earth's surface, with an ionization loss of approximately $-2\text{MeV/g/cm}^2 \approx -0.3\text{MeV/m}$ at STP [7]. This is sufficient to stop low-energy muons, implying that the muon flux at Earth's surface is dependent on atmospheric traversal length, and thus zenith angle. Thankfully, cosmic rays have isotropic flux in space near Earth,[3] so any surface-level angular distribution will be due to atmospheric effects.

## 2.2 Relativistic Effects

With a mean lifetime of $2.2\mu$s, it is a consequence of special relativity that we measure muons on the surface at all: if muons were not time-dilated,[4] they would have experienced at least $(2.2\mu\text{s})c/\ln(2) \approx 22$ half-lives by the time they reached the surface, reducing their count by a factor of 4 million. Meanwhile, we can easily find the Lorentz factor of a muon with kinetic energy $E$:

$$E = m_\mu c^2(\gamma - 1) \implies \gamma = \frac{E}{m_\mu c^2} + 1 \tag{3}$$

Muons have a mass of roughly $0.1\text{GeV/c}^2$ [9], so a muon with a typical kinetic energy of 1GeV will have an appreciable Lorentz factor of $\gamma = 11$, reducing the number of half-lives it experiences in its flight to just 2. This is why we observe a significant muon flux on the Earth's surface. Confirmation of this time-dilation served as an important milestone in the validation of special relativity in the 1940 Rossi-Hall experiment [12].

## 2.3 Analytical Model

Consequently, to even produce a simple model of muon flux at Earth's surface, both decay and energy-based losses must be considered. This is achieved in section 6.3 of Gaisser's book, *Cosmic Rays and Particle Physics* [7]. Ultimately, Gaisser reaches the result that:

$$I_\mu \propto (\cos\theta)^2 \tag{4}$$

[1] Cosmic ray muons have even been used to tomographically image the pyramids of Giza [11].

[2] The percentage of contribution to cosmic ray flux from different sources is still an open question.

[3] Though there is anisotropy in particles over $8 \times 10^{18}$eV [4].

[4] Alternatively, from the muon's frame, the atmosphere appears length-contracted.

That is, the energy-integrated muon flux $I_\mu$ is proportional to the squared cosine of the angle $\theta$ of the muon from the vertical axis (zenith angle). Additionally, the analysis finds that most surface-level muon energies are in the GeV range [7], which should make them deposit enough energy in our scintillators to be detectable.

### 2.4 Muon Decay

The dominant decay mode of the muon is [9]:

$$\mu^- \to e^- + \bar{\nu}_e + \nu_\mu \tag{5}$$
$$\mu^+ \to e^+ + \nu_e + \bar{\nu}_\mu \tag{6}$$

In this three-body decay, the daughter electron can at most carry away half the muon's invariant mass (≈53MeV) in kinetic energy [6]. This quantity is of the same order of magnitude as the energy we expect muons to deposit in our detectors as they pass through them; plastic has a density of roughly 1g/cm$^3$, and our scintillators are a few centimeters thick, so assuming ionization loss is ≈ 2MeV/g/cm$^2$, we expect a deposit of a few MeV in our detector.

Additionally, when a muon decays within our detector, the resulting electron will interact with the adjacent molecules in the scintillator, and ultimately release most of its energy radiatively. In other words, if we can detect muons passing through our detector, we can probably also detect them decaying.

## 3 Methodology & Procedure

### 3.1 Equipment

Our equipment chain consists of a QuarkNet Version 2 Data Acquisition (DAQ) board and two plastic scintillating paddles with QuarkNet photomultiplier tubes (PMTs) attached to them. Our measurements were taken near sea level (< 50m elevation) at the Florida Institute of Technology (28.1° N, 80.6° W). We set our PMT voltages to 1.40kV on both paddles. By attaching the QuarkNet board to a PC, we can use serial monitoring software to configure the board's trigger settings and record event timing information. We attached our paddles to the channels on the board via equal-length[5] LEMO cables connected to BNC adapters. We also use BNC tees to monitor our PMT signals on an oscilloscope (with proper termination).

When clearing its event buffer, the DAQ board sends its data in 16-word packets marking the rising and falling edges of observed pulses in each detector. The bulk of the data in these packets is timing information, which the board records with sub-clock precision (0.75ns resolution). We use a custom Python script to convert these rising and falling edges into ($t$, $\Delta t$) pairs of pulse start time and width, respectively.

When searching for coincidences, we look for pairs of pulses between detectors that occur within a 50ns window of each other. From the (2.3 counts/s) rate we will eventually identify, Poisson wait times of < 50ns only occur with a frequency of once every three months and will comprise just 0.00003% of total events − far from significance.

### 3.2 Muon Lifetime Measurement

We expect muon decay to follow an exponential decay distribution; that is, the amount of muons that decay in a time $\Delta t$ will be proportional to $e^{-\lambda_d \Delta t}$, where $\lambda_d = 1/\tau_d$ and $\tau_d$ is the mean lifetime of the muon [9].

We expect that, with low probability, a muon will occasionally deposit the bulk of its kinetic energy in our detector and decay while still inside it. Both the initial deposition of energy and the resulting decay will scintillate, resulting in two flashes separated by a decay time $\Delta t$.

Simultaneously, incoming (not necessarily decaying) muons strike our detectors in a Poisson process, which has a 'waiting time' distribution of the form $\lambda_p e^{-\lambda_p \Delta t}$, where $\lambda_p$ is the rate of incoming muons in counts per unit time.

If we record the delays between successive events in either of our detectors, we expect the number of delays in some interval $(t, t + \Delta t)$ to be distributed as follows:

$$N(t, t + \Delta t) \propto C e^{-\lambda_d t} + \lambda_p e^{-\lambda_p t} \tag{7}$$

Where $C$ is a constant determined by the probability of a decay occurring within a detector. Because we expect $\lambda_d$ to be much greater than $\lambda_p$ (muon lifetime is on the order of microseconds, while events occur at just a few hertz), instead of creating a histogram of raw time values, we instead create a histogram in $x = \ln(t)$ with constant bin size in $x$. This transform affects an arbitrary distribution $N(t)$ in the following way:

$$\frac{dN(t)}{dt} \to \frac{dN(t)}{dx} = \frac{dN(e^x)}{d\ln t} = \frac{dN(e^x)}{(1/t)dx} = t\frac{dN(e^x)}{dx} \tag{8}$$

That is, with sufficiently many bins, an arbitrary distribution $N(t)$ will become $e^x N(e^x)$. Applying this to a generic exponential distribution $N(t) = e^{-\lambda t}$ gives:

$$e^x N(e^x) = e^{x - \lambda e^x}. \tag{9}$$

This has the unique property that:

$$\frac{d}{dx} e^{x - \lambda e^x} = 0 \implies x = \ln\left(\frac{1}{\lambda}\right) = \ln(\tau) \tag{10}$$

In other words, we can identify the time constant of our distribution (e.g. the mean lifetime of the muon) simply by measuring the peak of its log-histogram. Furthermore, this method allows us to clearly separate the Poisson and decay

[5] This is important for coincidence detection; different-length cables could introduce a spurious delay in pulse arrival times.

distributions present in our data. This can be done per-detector, removing any need to only select multi-detector coincident events.

Because the Poisson process dominates our statistics, we analyze our data by fitting equation 9 to our data, recovering $\lambda_p$, then subtracting out the result from the histogram. We then reapply the fit (after visually selecting an appropriate range of data to fit) and identify $\lambda_d$.

## 3.3 Muon Telescope

### Notation and Monte-Carlo

The purpose of creating a muon telescope is to measure the angular flux[6] of cosmic-ray muons, $f$, with units $\mathrm{m}^{-2}\mathrm{s}^{-1}\mathrm{sr}^{-1}$:

$$f(\theta,\phi) = \frac{dR(\theta,\phi)}{d\Omega} = \frac{\#\text{ of muons}}{(\text{time})(\text{area})(\text{solid angle})} \tag{11}$$

For some differential muon flux $dR$ and differential solid angle $d\Omega = (\sin\theta)(d\theta)(d\phi)$. Like any experiment in particle physics, we cannot measure $f(\theta,\phi)$ directly. With our setup, we can only measure the *total* count and coincidence rates for a given detector angle. For a single detector with area $A$ and efficiency $\eta$ oriented in configurations that are can be rotated to the angle $(\theta,\phi)$ by an angle of $\Phi_i(\theta,\phi)$, we can make measurements $y_i$:

$$y_i = \eta A \int_\Omega f(\theta,\phi)(\cos\Phi_i(\theta,\phi))d\Omega \tag{12}$$

Where $\Omega$ is the upper hemisphere. These single-detector measurements are actually sufficient to inform us of the zenith-angle muon flux, but our results are improved by looking for coincidences with a second detector. This yields measurements of the form[7]:

$$z_i = \eta_1\eta_2 \int_\Omega f(\theta,\phi)S_i(\theta,\phi)d\Omega \tag{13}$$

Where $S_i(\theta,\phi)$ is the projected area of the overlap between the two detectors when viewed from the angle $(\theta,\phi)$. For our complex detector shapes, we determine $S_i$ using a GPU-accelerated numerical integration method.

Our detector geometry can be modelled as the union of a two primitives: a box and a trapezoid. To find $S_i$, we render these two solids from a specific $(\theta,\phi)$ using a virtual orthographic camera, and count the number of overlapping pixels. By carefully recording camera projection matrices, we can estimate the projected overlap from pixel count. Thankfully, it is only necessary to compute $S(\theta,\phi)$ for a vertically-oriented detector, after which all $S_i$ are obtained by rotating the resulting distribution to the detector's specific angle.

[6]This does not mean 'the flux through a plate held at some angle', but instead refers to muons travelling *at some specific angle.*

[7]We assume that muons travel in a straight line and are not significantly deflected by detector geometry. Given that our detectors are just a few cm thick, this is a safe assumption.

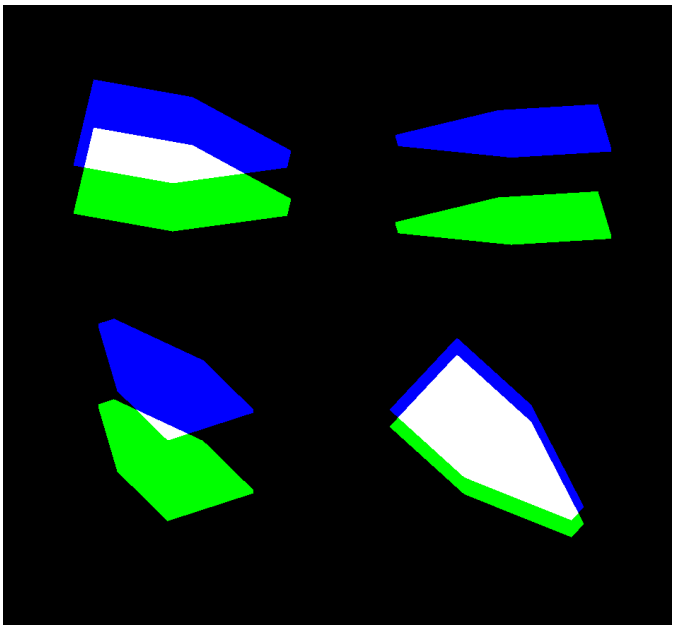

Figure 1: Examples of detector geometry viewed from various $(\theta,\phi)$. $S_i$ is recoverable from white pixel count.

This task is well-suited to typical computer graphics hardware. For efficiency, we implement this calculation in OpenGL Shading Language (GLSL) running on a consumer-grade GPU. We were able to simulate approximately $512\times512 \approx 2.6\times10^5$ rays for each of the $6.2\times10^4$ different angles sampled, making any potential error due to integration negligible. Simulating these $1.6\times10^{10}$ rays took just under ten minutes on an NVIDIA RTX3060 graphics card.

### Deconvolution

We are now ready to investigate the problem of recovering $f(\theta,\phi)$ from our measurements. First, we generalize the previous equations for rate measurements $x_i$:

$$x_i = \int_\Omega f(\theta,\phi)G_i(\theta,\phi)d\Omega \tag{14}$$

Where $G_i$ is either $\eta_1\eta_2S_i$ or $\eta A\cos\Phi_i$, depending on whether the measurement is triggering on singles or coincidences. Mathematically, this is an inner product between the angular flux $f$ and set of basis[8] angular flux distributions $G_i$. At this point, a naive way to reconstruct $f$ would be to take a simple linear combination of the basis $\{G_i\}$. But this would ignore the assumed constraint that $f = f(\theta)$. Instead, we let:

$$f(\theta,\phi) = \sum_i c_i h_i(\theta) \tag{15}$$

[8]Note that $B$ is by no means a *complete* or even *orthogonal* basis for the hemisphere.

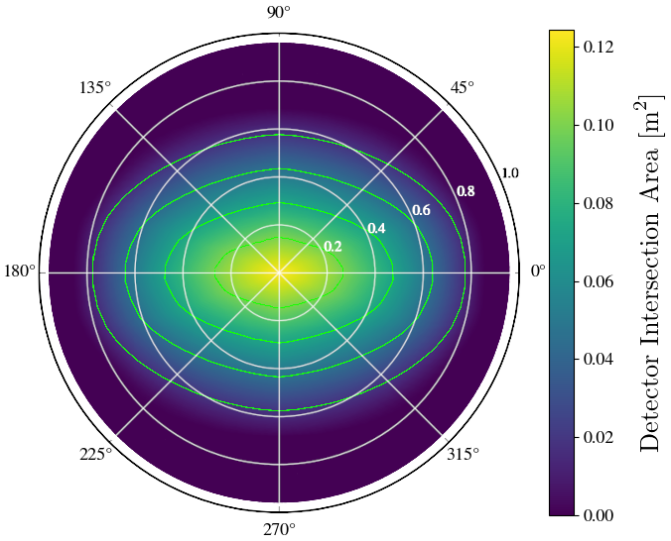


Figure 2: The projected intersection area of two vertically stacked detectors separated by 27.0 cm as a function of $\theta$ and $r = \sin^{-1}(\phi)$. Contour lines are shown in bright green.

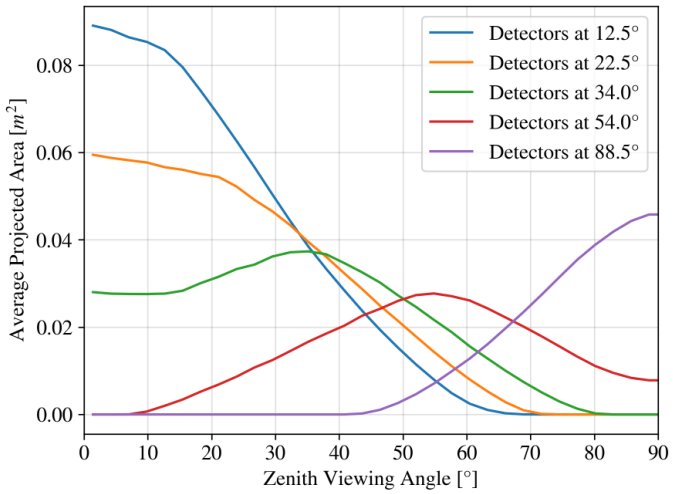


Figure 3: A plot of the 'detector basis': $\phi$-averaged projected intersection area as a function of viewing/incident muon angle for different telescope angles.

In other words, we write $f$ in some arbitrary univariate basis $\{h_i\}$ with components $c_i$. From here, we can employ simple linear algebra:

$$x_i = \int_\Omega \left( \sum_j c_j h_j(\theta) \right) G_i(\theta, \phi) d\Omega \tag{16}$$

$$= \sum_j c_j \int_\Omega h_j(\theta) G_i(\theta, \phi) d\Omega \tag{17}$$

$$= \sum c_j \mathbf{M}_{ij} \tag{18}$$

$$\implies \vec{x} = \mathbf{M}\vec{c} \tag{19}$$

$$\implies \vec{c} = \mathbf{M}^{-1}\vec{x} \tag{20}$$

Where $\mathbf{M}$ is the matrix taking us from the $\{G_i\}$ basis to the $\{h_i\}$ basis, and can be found via numerical integration over the hemisphere. In practice, applying this inversion yields unstable results when any kind of error is present in the input values. To compensate, we use a regularization technique to calculate $\vec{c}$ similar to Tikhonov regularization [8], but with a curvature-based penalty term. That is, instead of inverting $\mathbf{M}$, we find $\vec{c}$ by minimizing the quantity:

$$C(\vec{c}, \alpha) = ||\vec{x} - \mathbf{M}\vec{c}||^2 + \alpha \int_\Omega \left[ \frac{d^2}{d\theta^2} \left( \vec{c} \cdot \vec{h}(\theta) \right) \right]^2 d\Omega \tag{21}$$

If $\alpha = 0$, this has a minimum at $\vec{c} = M^{-1}\vec{x}$, but we add the second term to penalize curvature in our flux distribution and necessarily avoid wild, unphysical solutions.

We determine our regularization hyperparameter $\alpha$ via L-curve analysis: a method that finds the point of maximum curvature in the $\log(\alpha)$-parameterized cost function defined in equation 21 [8]. This method of solving inverse problems via regularization is sometimes referred to as *unfolding* or, in this specific case, *deconvolution*, and we will use these terms interchangeably for the remainder of this report.

Although we only apply unfolding to coincidences between detectors, we stress that the procedure described above can be applied to *any* set of detector configurations. In fact, with sufficient statistics, it would even be possible to create a rudimentary muon telescope with just one detector.[9]

Now we simply need to pick a basis $\{h_i\}$. We considered a few options:

1. Flat window functions in $\theta$ and $\cos\theta$.
2. Triangular window functions in $\theta$ and $\cos\theta$.
3. Even Legendre polynomials in $\cos\theta$ (the odd terms integrate to 0 because $f(\theta) = f(\pi - \theta)$).
4. The 'detector basis', i.e., $\{G_i(\theta, \phi)\}$ averaged over $\phi$.

Ultimately, the 'detector basis' yielded the most stable results and was easiest to integrate over. Our results follow below.

[9]The basis functions $G_i(\theta, \phi)$ for orientations of any asymmetric detector must be linearly independent, meaning counts from different single detector orientations are (in theory) sufficient to infer something about $f(\theta)$.

# 4 Results & Analysis

## 4.1 Absolute Flux

First, we convinced ourselves that our scintillator detectors were, in fact, detecting muons. We took data over three trials: one in which the detectors were stacked, another in which they partially overlapped, and a third where they were completely separate. The results of this confirmation

| Overlap Amount | Complete | Decreased | None |
|---|---|---|---|
| Time [h] | 47.8 | 0.94 | 118.0 |
| $dN(\text{Singles})/dt$ [$s^{-1}$] | 1.22 | 0.638 | 1.69 |
| $dN(\text{Coinc.})/dt$ [$s^{-1}$] | 0.15 | 0.043 | 0.0074 |
| Coinc./Singles | 0.12 | 0.068 | 0.0044 |
| Flux [$\text{min}^{-1}\text{cm}^{-2}$] | 0.059 | 0.031 | 0.081 |

Table 1: Single and coincidence count rates for our detectors in different overlapping configurations. Here, "singles" refers to the *average* number of single events detected, and flux was determined from singles rates. Counting errors are all $< 1\%$ and have been omitted from the table.

are tabulated above in table 1. Clearly, decreasing the detector's overlap results in a lower fraction of coincidences occurring. This indicates that whatever we are detecting, it is able to pass through both detectors in less than 50ns. In other words, the scintillators are probably responding to muons.

Meanwhile, our calculated fluxes (which were calculated assuming all muons 'see' the full detector surface area of $0.125\text{m}^2$) differ greatly from the expected value of 1 $\text{min}^{-1}\text{cm}^{-2}$, and are not even consistent across measurement. This is, in part, because we were still tuning our PMT settings between these measurements. We will address our setup's inconsistent efficiency in the following sections. Regardless, these measurements suggest that our detector's efficiencies generally lie somewhere between 1% and 10%.

## 4.2 Muon Lifetime

Using $4.99 \times 10^6$ events aggregated from a cumulative 163.8 hours of detector operation, we collected over 2000 probable decay events. Employing the methods used in 3.2 and 512 bins in $\ln(t)$, we find a muon mean lifetime of $(2.205 \pm 0.062)\mu$s, with error computed from our curve fit's output covariance matrix. This result agrees with the literature value of $2.196981(22)\mu$s [9] with an accuracy of 99.7% and a discrepancy of $0.12\sigma$. A log-log histogram of the intervals between successive events in our data is shown in figure 4. To collect as much data as possible, we include data from all experiments without restriction (including

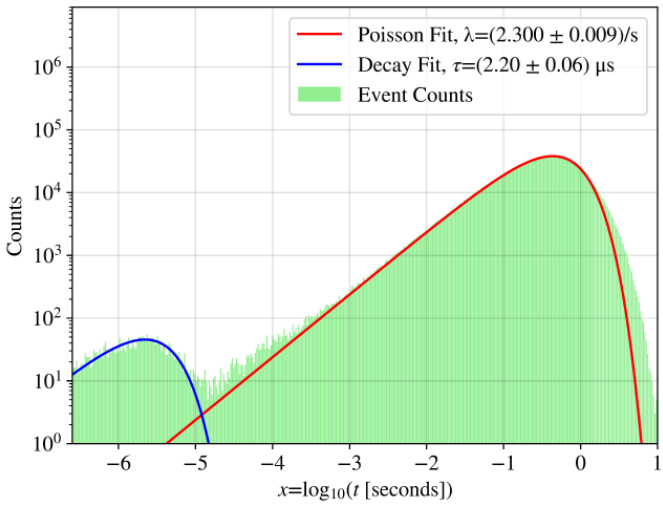


Figure 4: A histogram of time intervals between successive events with fits shown. Note that *both* the x and y-axes are log-scaled.

telescope measurements). When combined with higher-altitude data [5], our result clearly refutes the relativistic null hypothesis.

## 4.3 Detector Efficiency

Due to the high noise floor of our PMTs, our detectors operated at a fairly low efficiency of just a few percent. That is, if a hundred particles pass through our detector, only a few of them will result in a trigger on the DAQ board.

Unfortunately, accurately measuring this efficiency is a challenging task. Ideally, we would place both detectors directly on top of each other and compute the efficiency $\eta = (\#\text{ of singles}/\#\text{ of coincidences})$. However, when both detector boxes are sitting on top of each other, there is still a 9.5mm gap between the two scintillators, and some muons may travel through one detector but not the other. Determining what fractions of muons can do this requires that we know $f(\theta, \phi)$, and we find that we cannot precisely determine $\eta$ without either *a priori* knowledge of $f(\theta, \phi)$, or data from an external source. To resolve this, we find $\eta$ by numerically integrating to compute coincidence-single ratios using some $\eta$ and $f(\theta)$, then comparing these values to the actual measurements and finding a new $\eta$. We attempt to search for $\eta$ that make the distribution self-consistent (i.e. are invariant under this iterative transform). Our initial guess is informed by the classical $\cos^2\theta$ distribution, but we do not expect our results to be heavily influenced by this assumption.

We find that our average detector efficiency during the telescope trials was (9.0±1.5)%. The large variation in this rate across detector configurations is due to the high

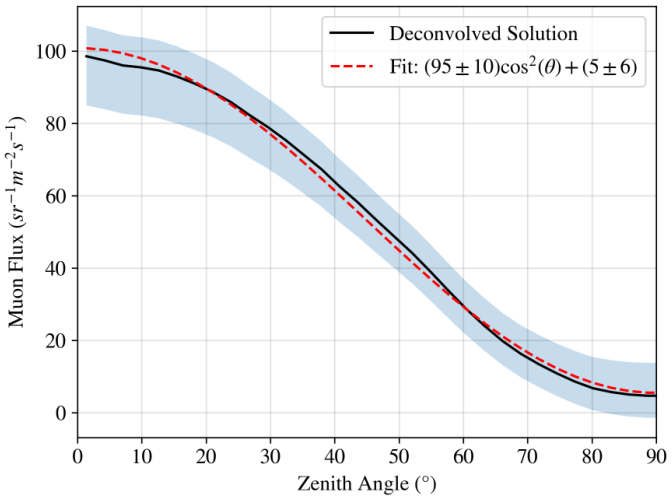


Figure 5: Our final deconvolved zenith angle muon flux measurement. Despite uncertainty in its magnitude, the result matches the expected $\cos^2(\theta)$ distribution very well, with some constant offset. A $1\sigma$ margin of error propagated from uncertainty in choice of $\alpha$ and uncertainty in $\eta$ is shown in blue.

sensitivity of our PMTs to bumps and movement: every small shift of the telescope seemed to affect our count rate.

### 4.4 Muon Telescope

We separated our detectors by (270±1)mm and held them at zenith angles of 12.5°, 22.5°, 34°, 54°, and 88.5° for a cumulative 50 hours[10]. Using our computed efficiency, we use the process described in section 3.3 to unfold our data in the detector basis and recover muon flux as a function of zenith angle.

Unfortunately, our results are highly uncertain in magnitude (absolute flux) due to the lack of accuracy with which we can measure our detector efficiency, as well as the uncertainty in our regularization parameter $\alpha$. However, the *shape* of our distribution is unaffected by variations in $\eta$ and relatively unaffected by variations in $\alpha$ around the L-curve identified value. We find that this function is well-fit ($R^2 > 0.997$) by a $\cos^2(\theta)$ distribution, as shown in figure 5.

From this fit, we calculate a vertical muon flux of $(95 \pm 10)$ $s^{-1}m^{-2}sr^{-1}$ with a constant offset of (5±6) $s^{-1}m^{-2}sr^{-1}$. We attribute this offset to our regularization restriction that all fluxes must be positive, and the inability of the basis functions to exactly replicate the desired distribution. Our final value of $I_0 = (95 \pm 10)$ $s^{-1}m^{-2}sr^{-1}$ is in good agreement with the literature sea-level rate of ≈100 $s^{-1}m^{-2}sr^{-1}$ [3].

[10]The majority of time was spent in the near-horizontal 88.5° because counts were low.

## 5 Conclusion

After confirming that our detectors were responding to muons, we measured a muon lifetime of (2.205±0.062)$\mu$s by curve-fitting a log-log histogram of waiting times between detector pulses. This result agrees with literature to an accuracy of 99.7%. Next, we characterized the efficiency of our detectors and determined that the vertical muon flux at our detectors was $(95 \pm 10)$ $s^{-1}m^{-2}sr^{-1}$. We achieved this result via a curvature-regularized data analysis. We see that our result matches the expected $\cos^2\theta$ distribution but also includes a constant offset, indicating a possible systemic error. We attribute this error primarily to the details of the unfolding process. Finally, we include details of an anomalous observation described in appendix A. We end by noting that all analysis source code is available online [10].

# Bibliography


[1] Johannes Albrecht, Lorenzo Cazon, Hans Dembinski, Anatoli Fedynitch, Karl-Heinz Kampert, Tanguy Pierog, Wolfgang Rhode, Dennis Soldin, Bernhard Spaan, Ralf Ulrich, and Michael Unger. The muon puzzle in cosmic-ray induced air showers and its connection to the large hadron collider. *Astrophysics and Space Science*, 367(3), March 2022.

[2] D.J. Bird, Steven Corbato, H. Dai, Jerome Elbert, Kevin Green, Ming-Huey Huang, Seb Ko, Curtis Larsen, E. Loh, May Luo, M. Salamon, J. Smith, Pierre Sokolsky, P. Sommers, J. Tang, and S. Thomas. Detection of a cosmic ray with measured energy well beyond spectral cutoff due to microwave radiation,. *The Astrophysical Journal*, 441:144–150, 03 1995.

[3] Cristian Borja, Carlos Ávila, Gerardo Roque, and Manuel Sánchez. Atmospheric muon flux measurement near earth's equatorial line. *Instruments*, 6(4), 2022.

[4] The Pierre Auger Collaboration. Observation of a large-scale anisotropy in the arrival directions of cosmic rays above 8 × 10 18 ev. *Science*, 357(6357):1266–1270, September 2017.

[5] S Coutu, JJ Beatty, MA DuVernois, SW Barwick, E Schneider, A Bhattacharyya, CR Bower, JA Musser, A Labrador, D Müller, et al. Energy spectra, altitude profiles, and charge ratios of atmospheric muons. *Physical Review D*, 62(3):032001, 2000.

[6] Andrzej Czarnecki, Matthew Dowling, Xavier Garcia i Tormo, William J Marciano, and Robert Szafron. Michel decay spectrum for a muon bound to a nucleus. *Physical Review D*, 90(9):093002, 2014.

[7] Thomas K Gaisser. Cosmic rays and particle physics. *Comments on Nuclear and Particle Physics*, 11(1):133, 2016.

[8] Gene H Golub, Per Christian Hansen, and Dianne P O'Leary. Tikhonov regularization and total least squares. *SIAM journal on matrix analysis and applications*, 21(1):185–194, 1999.

[9] Particle Data Group. Review of Particle Physics. *Progress of Theoretical and Experimental Physics*, 2020(8):083C01, 08 2020.

[10] Adam Lastowka. muon-analysis. https://github.com/Rachmanin0xFF/muon-analysis.

[11] Sébastien Procureur, Kunihiro Morishima, Mitsuaki Kuno, Yuta Manabe, Nobuko Kitagawa, Akira Nishio, Hector Gomez, David Attié, Ami Sakakibara, Kotaro Hikata, et al. Precise characterization of a corridor-shaped structure in khufu's pyramid by observation of cosmic-ray muons. *Nature Communications*, 14(1):1144, 2023.

[12] Bruno Rossi and David B Hall. Variation of the rate of decay of mesotrons with momentum. *Physical Review*, 59(3):223, 1941.

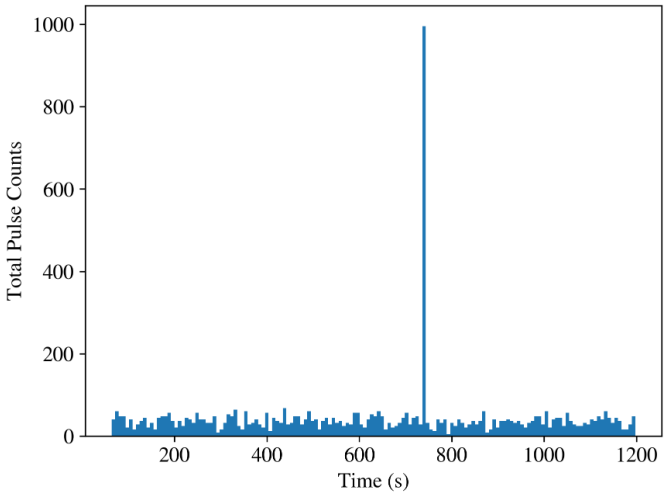


Figure 6: The strange burst of pulses identified in the dataset.

# 6 Appendix A: Anomalous Event

We observed an unusual spike in our data while the detectors were completely separated. The rapid barrage of pulses is shown in figure 7; we recorded approximately 1000 pulses in a single second.

Strangely, these pulses were split across three separate bursts separated by over 200ms. Each of these sub-bursts occurs over the span of roughly 2ms. The actual pulses within the bursts show no obvious pattern between detectors. Given that the three bursts span nearly a full second, it seems unlikely that this is a cosmic ray shower. We suspect that the anomaly has some electrical origin in the DAQ system, though we are not sure exactly what. Additionally, we note that both experimenters were far from both detectors when this event occurred.

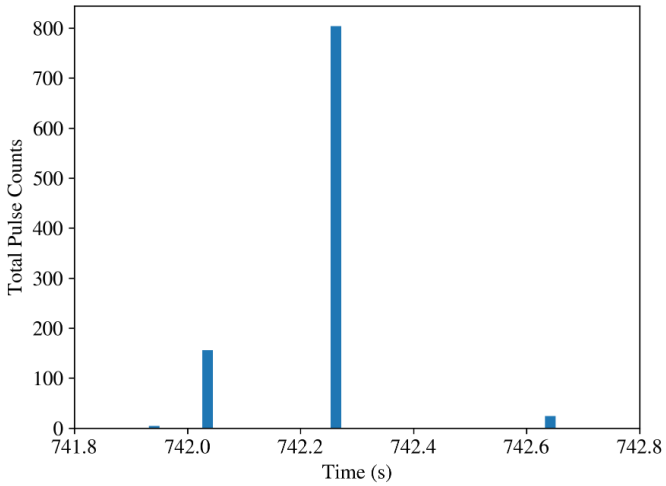


Figure 7: Detail of the burst.